www.czasopisma.pan.pl PAN POLSKA AKADEMIA NAUK www.journals.pan.pl

Arch. Min. Sci. **71** (2026), 1, 79-102

Electronic version (in color) of this paper is available: http://mining.archives.pl

DOI: https://doi.org/10.24425/ams.2026.157757

CHEN LI[1], XINZHU HUA[1,2], PENG YANG[1,2*], XIAO LIU[3], JIYUAN YAN[1]

STRUCTURAL EVOLUTION AND STRESS TRANSFER MECHANISMS OF THE FLOOR IN DEEP ROOF-CUTTING GOB-SIDE ENTRY RETAINING

Based on the engineering background of (1) roof-cutting and retaining roadway working face in Dingji Coal Mine of Huainan, the stress characteristics of the floor and the stress transfer mechanism caused by mining in the process of retaining roadway are studied. The stress in the roadway and the roadway after roof-cutting is relieved, and the floor stress is symmetrically distributed. During the first mining period, the stress at 5 m of the roadway side is concentrated, and the high stress is transmitted to the floor through the coal body. The stress on the solid coal side is restored, and the large-scale pressure relief on the goaf side forms an asymmetric stress field. The vertical stress is transmitted to the floor through the 'short cantilever' structure of the roof, and the 'short cantilever' structure is characterised by high tension and low compression. As the gangue collapses, the bending subsidence of the overburden rock causes the key parts of the roof to rotate and sink, and the high additional load is transmitted to the floor through the coal side and the supporting body in the roadway, resulting in an increase in the stress on the floor of the retained roadway. After the goaf is compacted, the floor fully touches the gangue and shares the load with the key parts of the coal body and the roof.

Keywords: Roof-cutting retaining roadway; physical similarity simulation; floor stress deformation; floor stress transfer

[1] ANHUI UNIVERSITY OF SCIENCE AND TECHNOLOGY. STATE KEY LABORATORY FOR SAFE MINING OF DEEP COAL RESOURCES AND ENVIRONMENT PROTECTION, HUAINAN, 232001, ANHUI, CHINA

[2] ANHUI UNIVERSITY OF SCIENCE AND TECHNOLOGY. JOINT NATIONAL-LOCAL ENGINEERING RESEARCH CENTRE FOR SAFE AND PRECISE COAL MINING, HUAINAN, 232001, ANHUI, CHINA

[3] CHINA COAL TECHNOLOGY AND ENGINEERING GROUP SHENYANG RESEARCH INSTITUTE, STATE KEY LABORATORY OF COAL MINE SAFETY TECHNOLOGY, FUSHUN, 113000, LIAONING, CHINA

* Corresponding author: pyangaust@126.com

1. Introduction

The roof-cutting self-formed roadway technology eliminates the need for constructing filling bodies beside the roadway and offers significant technical and economic advantages in terms of increasing the recovery rate and reducing the amount of roadway excavation [1,2]. Physical similarity simulation is widely used to study the deformation and failure patterns of surrounding rock in gob-side entry, as well as the evolutionary characteristics of overlying rock structures. It can reveal general laws such as the stress distribution and displacement evolution of the surrounding rock in retained roadways, providing certain guidance for on-site roadway support [3]. The gob-side entry has a long service life, and it will experience the influence of excavation and two strong mining operations. The surrounding rock undergoes severe deformation and failure, creating a large plastic zone. Almost all gob-side entries experience varying degrees of floor heave, and as the burial depth increases, the floor heave problem becomes more pronounced [4-6]. After roadway excavation, the floor undergoes immediate unloading, leading to an increase in internal fissures within the rock mass and overall failure. Under the high pressure of the roadside support, the rock mass slips towards the floor, initiating the formation of floor heave [7,8]. During the excavation period, the floor heave is not significant, with the floor deformation symmetrically distributed and the maximum heave located at the centre of the roadway. In the stage of primary mining and retaining roadway, the floor heave of the roadway is the largest, exhibiting an asymmetric distribution with the maximum heave biased towards the gob side. In the secondary mining stage, affected by the superposition of two mining stages, the floor heave of the roadway in the advance working face is more severe. Research indicates that significant floor deformation primarily occurs during mining extraction and in the retained roadway, with roof pressure being the fundamental cause of floor heave [9-11]. This is attributed to the dynamic load from the collapse of the overlying strata, which is transmitted to the floor via the coal ribs and support structures [12,13]. Additionally, the lateral pressure generated in the floor beneath the compacted goaf and the solid coal after compression is the direct cause of floor heave [14,15]. The pressure from the roof and overlying strata is transmitted to the floor through the solid coal ribs, support structures, and the goaf. Consequently, the floor rock mass is subjected to lateral squeezing forces from both sides, leading to its release towards the free face and resulting in significant floor deformation [16-18]. Top-cutting can weaken the transmission of stress above the roadway, thereby improving the stress environment of the surrounding rock in the roadway. Compared to the state without top-cutting, the failure depth of the floor and the amount of floor heave are significantly reduced. Therefore, the rational design of top-cutting parameters and the selection of top-cutting methods are particularly important for the stability of the surrounding rock in the roadway [19-21]. After top-cutting, as the mining area of the coal seam increases, the lower overlying strata break and collapse, while fractures develop in the higher overlying strata. The roof collapses along the pre-cut slots under the mining pressure, automatically forming the roadway ribs. The overlying strata in the goaf undergo rotation, subsidence, separation, and fracturing under self-weight stress, and exhibit periodic breaking behaviour. Ultimately, both the mining-induced fractures and the collapsed structure of the overlying strata take on a 'trapezoidal' shape [22,23]. Different top-cutting parameters result in varying manifestations of mine pressure in the roadway. It is commonly held that the top-cutting height is reasonable when the main roof fractures along the pre-cut line [24]. At this point, the collapse of the goaf roof does not impose a compressive effect on the roadway's surrounding rock, leading to a notable pressure relief effect. When the angle α between the top-cutting and the vertical plane of the roof is less than

10°, the friction between the 'short-arm beam' structure and the goaf roof is significant, leading to poor collapse performance of the roof strata. Conversely, when the top-cutting angle is too large, the length and weight of the 'short-arm beam' structure increase, which is detrimental to the stability of the roadway [25-27].

The aforementioned studies have made significant progress in elucidating the mechanism of roadway floor heave, the deformation patterns of the floor, and the effects of pressure relief through roof-cutting, thereby providing a crucial theoretical foundation for the stability control of gob-side entry retaining. However, roadway floor heave remains an extremely complex engineering challenge influenced by a multitude of factors. The floor heave of the retained roadway mainly occurs during the period from primary mining to the retained roadway, which affects the stability of the retained roadway and restricts the roadway repair and the safe mining of the working face in the lower section. The existing research on roof-cutting and retaining roadway mostly focuses on roof pressure relief, and there are few studies on floor heave. The research on the evolution characteristics and stress transfer path of the floor structure of deep mine roof-cutting and retaining roadway is not sufficient, and the understanding of the floor structure of gob-side entry and the stress transfer path and floor force source of surrounding rock after roof-cutting is insufficient. Therefore, the purpose of this paper is to further reveal the evolution characteristics and stress transfer path of the floor structure of deep mine roof-cutting and retaining roadway through physical similarity simulation test combined with numerical calculation and engineering field practice, so as to provide new ideas and methods for the stability control of surrounding rock of deep mine roadway.

2. Physical similarity simulation test of deep mine roof-cutting entry retaining

2.1. Engineering geology

The 1452(1) working face of the Dingji Coal Mine in Huainan is situated at elevations ranging from –908 m to –931 m, with a maximum overburden depth of 950 m. It features a strike length of approximately 800 m and a dip length of 180 m. The coal seam exhibits a nearly horizontal orientation, with a mining height varying between 2.9 m and 4.3 m, averaging 3.6 m. The mining operation proceeds from west to east, with pre-splitting and roof-cutting technology implemented 30 meters ahead of the working face. The transport roadway of the 1452(1) working face is retained to serve as the track roadway for the 1462(1) mining working face (referred to as the 1462(1) track roadway in this paper), thereby achieving pillarless mining. The principle of roadway retention technology is illustrated in Fig. 1, and the columnar structure of coal and rock is shown in Fig. 2. The physical similarity simulation is based on the Huainan Dingji Coal Mine 1452(1) roof-cutting and roadway retention working face, with relevant parameters derived from the geological data of the 1462(1) track roadway.

2.2. Similarity Principle and Similar Materials

Based on the dimensions of the experimental model system and the known geological conditions of the field, and in accordance with the three fundamental theorems of similarity theory,

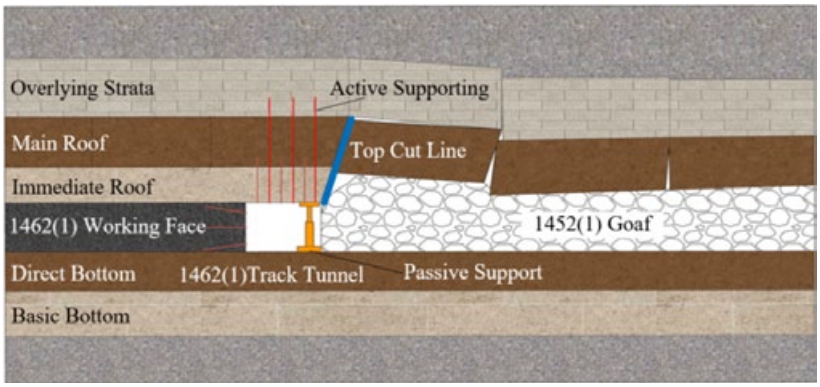

Fig. 1. Schematic diagram of the principle of roof-cutting and roadway retention technology in Dingji Coal Mine

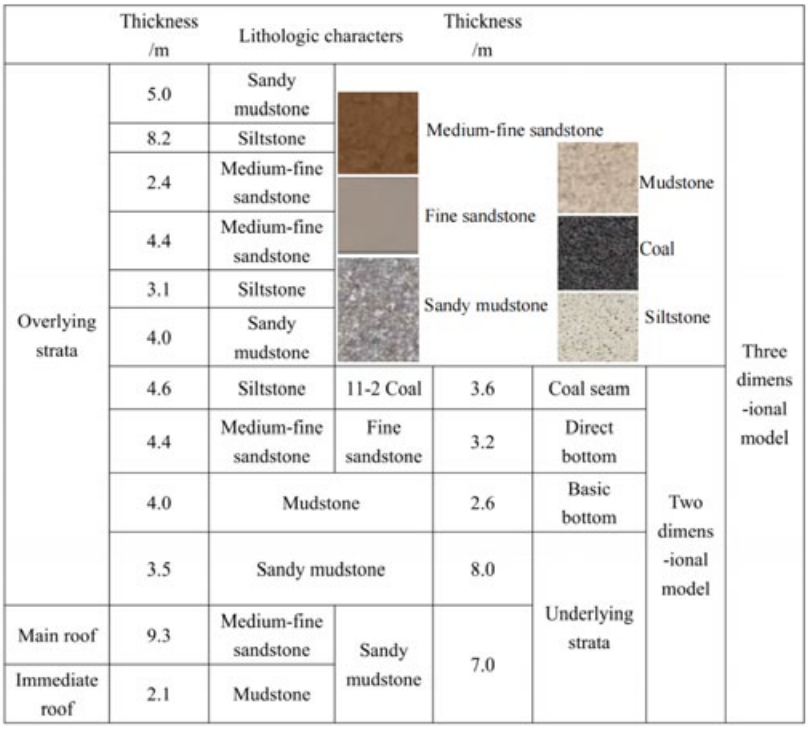

Fig. 2. Comprehensive histogram of rock strata

the geometric similarity ratio between the model and the prototype is selected as $C_L = 1/50$, the bulk density similarity ratio as $C_\gamma = 0.7$, the stress similarity ratio as $C_\sigma = 0.014$, and the time similarity ratio is such that, for ease of recording, every 3.6 hours in the model corresponds to one day and night in the field.

According to the physical and mechanical parameters of each rock stratum in the engineering site, combined with the similarity ratio, the physical and mechanical parameters of the rock corresponding to the test model can be obtained as shown in TABLE 1. Based on the analysis and summary of the current research status of similar materials, and in combination with the characteristics of the materials themselves, the author finally determined to use fine river sand (150 mesh) as the aggregate, lime and gypsum as the cementing materials, and to mix in a certain proportion of barite powder to adjust the material's density, mica powder as the interlayer interface, and based on previous experience and the dryness and wetness of the river sand, the water addition is 5% to 10% of the total solid mass. Based on the mechanical test of 1462(1) rail along lithology in Dingji Mine and related literature, standard specimens were prepared according to a certain process and mechanical tests were carried out. After screening and comparison, the content and ratio of each material were finally determined, as shown in TABLE 2. The production process of similar materials is shown in Fig. 3. The ratio number is P_1P_2-$P_3P_4P_5$, P_4:P_5 is the mass ratio of lime to gypsum, P_3 is the mass ratio of river sand to lime gypsum, P_1:P_2 is the ratio of the total mass of river sand, lime gypsum to barite powder, and 00 is not using barite powder.

TABLE 1

The content of similar materials in each rock layer and its ratio number

Lithologic characters		**Uniaxial strength (MPa)**	**Tensile strength (MPa)**	**Elastic modulus (GPa)**	**Cohesion (MPa)**	**Friction angle (°)**	**Density (kN/m^3)**
Sandy mudstone	Prototype	27.5	3.7	10.8	3.1	34	25.30
	Model	**0.550**	**0.074**	**0.216**	**0.062**	**34**	**25.30**
Medium-fine sandstone	Prototype	50.2	7.1	20.1	6.2	40	26.80
	Model	**1.004**	**0.142**	**0.402**	**0.124**	**40**	**26.80**
Mudstone	Prototype	14.2	1.9	7.5	1.6	30	24.70
	Model	**0.284**	**0.038**	**0.150**	**0.032**	**30**	**24.70**
11-2 Coal	Prototype	12.6	0.35	1.5	1.1	28	14.00
	Model	**0.252**	**0.007**	**0.030**	**0.022**	**28**	**14.00**
Fine sandstone	Prototype	43.8	5.3	18.5	5.2	38	26.10
	Model	**0.876**	**0.106**	**0.370**	**0.104**	**38**	**26.10**
Siltstone	Prototype	35.0	4.6	14.0	4.5	37	26.50
	Model	**0.700**	**0.092**	**0.280**	**0.090**	**37**	**26.50**

TABLE 2

The content of similar materials in each rock layer and its ratio number

Lithologic characters	**Proportion number**	**Quartz sand**	**Lime**	**Gypsum**	**Barite**	**Water**
Fine sandstone	121-411	73.5%	10.0%	9.0%	7.5%	5%~10%
Sandy mudstone	121-454	74.5%	10.0%	8.0%	7.5%	
Mudstone	151-521	78.5%	10.5%	5.0%	6.0%	
Medium-fine sandstone	545-375	70.0%	12.5%	9.0%	8.5%	
Siltstone	121-495	75.5%	11.0%	6.0%	7.5%	
11-2 Coal	000-673	70.0%	18.0%	12.0%	0.0%	

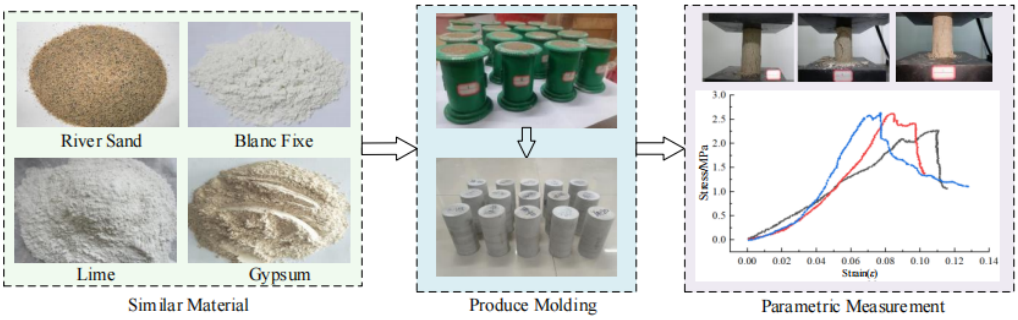

Fig. 3. Fabrication and testing of similar materials

3. Physical simulation experiment design

According to the main research contents of this paper, on the one hand, the spatial size of the roadway should be taken into account, and the deformation and failure characteristics of the floor of the roof-cutting roadway under the mining response should be presented more intuitively. On the other hand, the model size and the simulation range of the stope should be considered comprehensively, which can reflect the migration characteristics of the rock strata within a certain range. For this reason, this experiment designs two kinds of models, a three-dimensional model and a two-dimensional plane model.

3.1. Three-dimensional physical similarity model

3.1.1. Three-dimensional model constructing

The three-dimensional physical similarity model can more realistically restore the stress environment of the surrounding rock of the roadway, and can more intuitively present the deformation characteristics of the surrounding rock of the retaining roadway. Considering the length limit of the model and the boundary effect after pressure, the roadway is arranged at a 2/5 position of the coal seam. The roadway is 110 mm wide and 72 mm high. It is pre-buried with double-row double-layer 55 mm×36 mm×700 mm wooden strips. The top cutting line is pre-buried with a double-layer galvanised steel plate, 700 mm long, 236 mm wide and 1 mm thick. The wooden strip and the steel plate are drilled through the edge with an iron wire to facilitate subsequent extraction. In the process of roof-cutting into the roadway, the stack support on the roof-cutting side is an important force transmission carrier and roadway protection structure. According to the conditions of retaining roadway in the field, the stacking support model was made according to similar proportion. The top and bottom of the support and the column were composed of steel blocks and hollow steel pipes. The steel spring (Hook coefficient K = 1000 N/m measured in the laboratory) was used to splice the two steel pipes, so that the support had a certain degree of compressibility. The construction process of the bracket and the three-dimensional model is shown in Fig. 4 and Fig. 5.

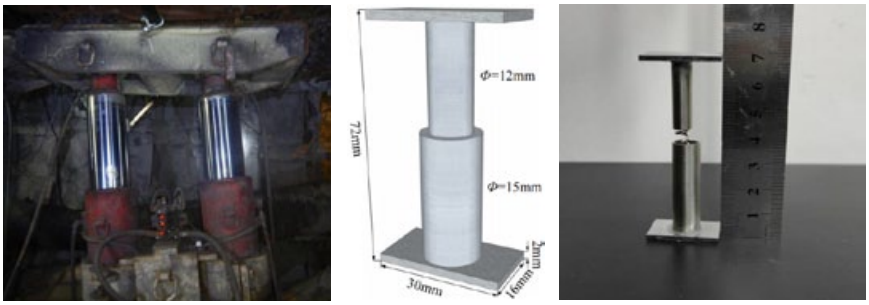

Fig. 4. Fabrication of Stacked Support in Roadway

Fig. 5. Three-dimensional physical model and production

3.1.2. Three-dimensional model loading device

The prototype buried depth of (1) track roadway in Dingji Mine is 950 m, In the physical model, the simulated buried depth at the top boundary is 913.2 m, whereas that at the bottom boundary is 970.5 m. and the simulated rock bulk density is 25.0 kN·m^3. Then the original rock stress at the upper part of the prototype is 22.83 MPa, and the original rock stress at the bottom of the prototype is 24.26 MPa. According to the stress similarity ratio of 0.014, the vertical stress of 0.32 MPa and the horizontal stress of 0.46 MPa are applied at the top of the model. The hydraulic cylinder diameter of the model is 140 mm, and the loading plate area is 0.105 m^2. The relationship between the set pressure and the pressure on the model is as follows: tubing pressure = (simulated in-situ stress value×loading plate area) / cylinder cross-sectional area. In the case of ignoring the friction resistance, the model loading value is shown in TABLE 3. Because the

TABLE 3

Loading data of hydraulic cylinder

Load Position	Dimension (m^2)	Depth of Embedment (m)	Actual Stress (Mpa)	Simulated Stress (MPa)	Tubing Pressure (Mpa)	Setting Pressure (Mpa)
Roof	0.105	913.2	22.83	0.32	2.74	2.74
Left Side	0.105	950.0	32.25	0.46	3.95	3.95
Right Side	0.105	950.0	32.25	0.46	3.95	3.95
Bottom	0.050	970.5	24.26	0.34	—	—

loading cylinder is not provided at the bottom of the three-dimensional similar model, the three-cylinder hydraulic head is arranged along the direction between the basic bottom and the direct bottom layer directly below the roadway, which is controlled by manual pressure and fixed with the floor (support plate size: 0.1 m×0.5 m) to provide a stable force source for the direct bottom.

3.2. Two-dimensional plane physical similarity model

3.2.1. Fabrication of two-dimensional plane physical model

Due to the limitation of the three-dimensional model's size, it is difficult to reveal the evolution law of the overlying rock structure after the roof-cutting. Therefore, a plane physical similarity model is established on the basis of the three-dimensional model to study the breaking and caving morphology and force transfer path of the overlying rock structure under the roof-cutting. At the same time, it is combined with the three-dimensional model to verify. The physical similarity simulation plane test bench with bidirectional four-sided loading is used to realise the four-sided stress loading of the model boundary. The materials and parameters selected by the model are the same as those of the three-dimensional model. The laying height of the rock layer is increased by 0.4 m on the basis of the three-dimensional model according to the coal-rock histogram. The model making process is shown in Fig. 6.

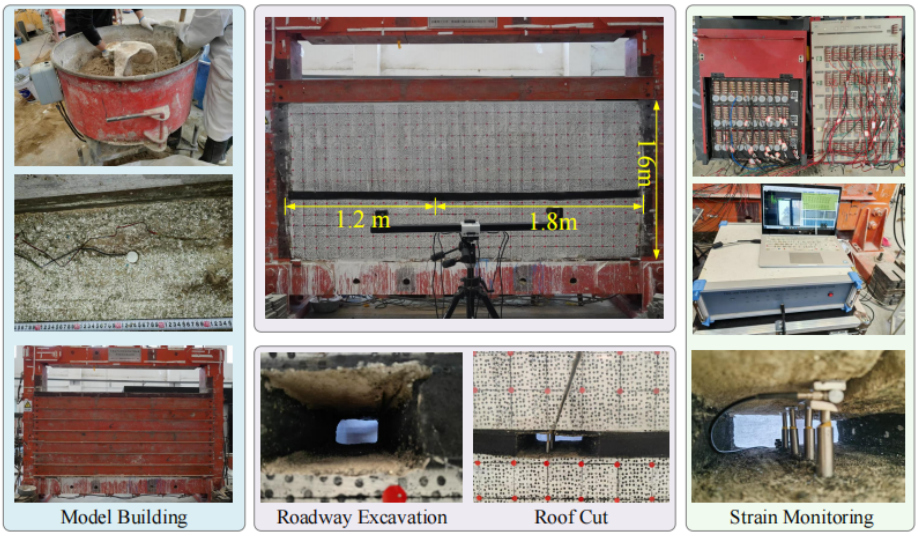

Fig. 6. Planar physical model and fabrication

3.2.2. Plane model loading device

The model loading system consists of 22 hydraulic loading units in 4 groups. The rated pressure of a single hydraulic pump is 28 MPa. The oil circuits of each group of loading units are connected in parallel and independently controlled by the hydraulic control system, which can continuously load, maintain pressure and unload with equal pressure. According to the calcula-

tion of 1462(1) rail along the buried depth of 950 m, the vertical stress of 0.32 MPa is applied at the top of the model, the horizontal stress of 0.45 MPa is applied in the horizontal direction, and the upward vertical stress of 0.34 MPa is applied at the bottom. The loading value of the plane model is shown in TABLE 4.

TABLE 4

Loading data of hydraulic pump station

Load position	Depth of embedment (m)	Actual stress (Mpa)	Simulated stress (Mpa)	Pumping station pressure (Mpa)
Roof	900	22.50	0.32	6.08
Both sides	950	32.25	0.45	8.55
Bottom	975	24.38	0.34	5.10

3.3. Test monitoring scheme

This paper mainly studies the process of stress deformation and stress evolution of the roadway floor structure during primary mining and roadway retention. Based on the design of model size, thickness of each rock layer, roadway size and length of working face, and according to the research content of this experiment, monitoring is mainly divided into two aspects. One is to monitor the stress and deformation characteristics of the surrounding rock of the three-dimensional physical model roadway, and the other is to monitor the rock movement and caving structure characteristics of the two-dimensional plane physical model. Fig. 7(a) shows the arrangement details of measuring points around the three-dimensional model roadway. There are two sections monitored in the direction of strike, namely A-A and B-B, and the direction of inclination starts from the direct bottom surface. According to the stratification, they are recorded as F_A1-7, F_B1-7, F_C1-5 and F_D1-5, respectively. The distance between each measuring point is 2.5 cm. Fig. 7(b) is a two-dimensional plane physical model monitoring diagram, and the speckle monitoring points are brushed on the surface of the model.

3.4. Model excavation steps

After the three-dimensional similar model is laid, it is naturally air-dried. After the model reaches the expected strength, the excavation of the project is simulated. The pressure set in TABLE 2 is the maximum value, and the step-by-step loading method is used to increase by 0.5 MPa every 0.5 h until the maximum value. After the model pressure is stable, the roadway and working face are excavated. The overall excavation is divided into three stages. The steps are as follows :

(1) TThe model is pre-loaded step by step before excavation, and the pressure is continuously stabilised for 12 hours. After the pressure reaches the preset value, the prefabricated wood strips are extracted to simulate the excavation of the roadway, and then the prefabricated iron sheets are extracted to simulate the roof-cutting process. After the roof-cutting is completed, the support is placed in turn on the top cutting side of the roadway as shown in Fig. 8(a).

(2) The upper section of the working face is excavated. The excavation of the three-dimensional model coal seam is divided into two directions: tendency and strike. Each time,

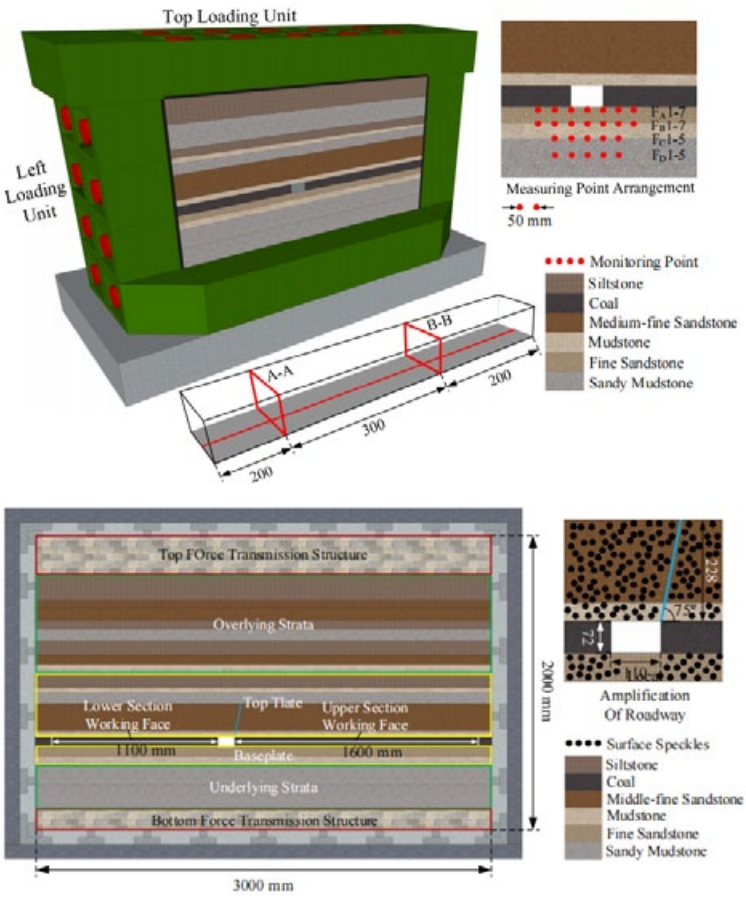

Fig. 7. Physical similarity model monitoring

900 mm is excavated along the tendency and 140 mm is excavated along the strike, as shown in Fig. 8(b). After each step of excavation is completed, it is allowed to stand for 20-30 min until the rock layer is stable, and then the next step of excavation is carried out. The plane model does not need to consider excavation in the strike direction and instead excavates 150 mm at a time along the dip direction of the coal seam, for a total of 11 excavations. As shown in Fig. 8(c), considering the boundary effect of the model, 10 cm boundary coal pillars are reserved in the coal seam.

After the excavation of the upper section working face, the excavation of the lower section working face is carried out, and the steps are the same. Since the secondary mining stage is not the focus of this study, the author does not elaborate on the stress and deformation of the surrounding rock of the roadway at this stage. Following the excavation and monitoring work, the test bench was cleaned, the data organised, and the experiment concluded. In order to more intuitively display the stress of the surrounding rock of the roadway, the strain value of the test model was uniformly converted into the actual stress value, measured in MPa.

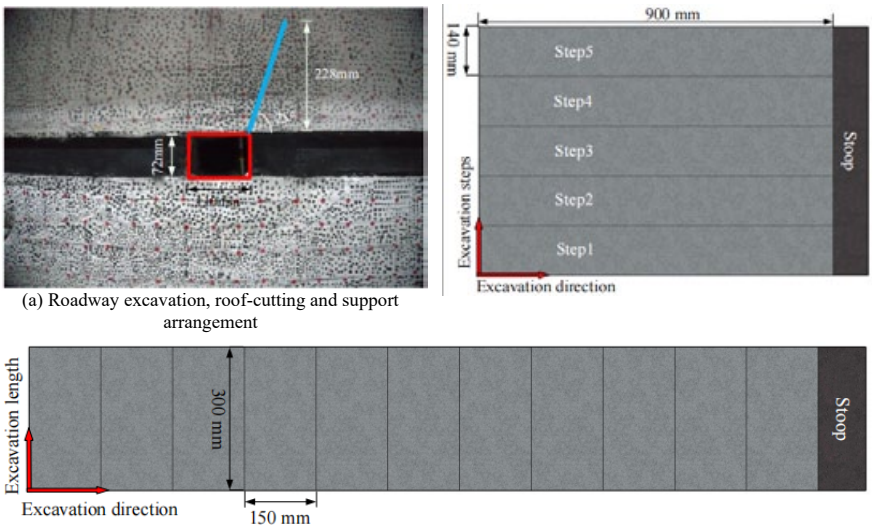

(a) Roadway excavation, roof-cutting and support arrangement

Fig. 8. Physical model of coal seam excavation

4. Characteristics of floor stress evolution in deep mines using roof-cutting for gob-side entry retaining

In accordance with the experimental design, prior to the test, the model was subjected to ground stress loading, involving continuous pressurisation to 23.5 MPa, followed by a stabilisation period of 12 hours. Subsequently, after completing procedures such as roof-cutting and support installation, the excavation of the working face commenced at the 3.25-day mark. The excavation process was conducted in a total of five steps, with each step involving the removal of a section measuring 900 mm in the dip direction and 140 mm in the strike direction. Immediately following the completion of each excavation step, the roadway transitioned into the retention stage.

4.1. Analysis of stress evolution of overlying strata

After the excavation of the roadway, the underlying rock strata experienced instantaneous unloading. As illustrated in Fig. 9, the vertical stress at each measurement point decreased uniformly to 18.5 MPa. The stress was then redistributed, resulting in a reduction of 5.0 MPa compared to the original in-situ stress. Due to the significant distance of the measurement points from the roadway surface and the minimal disturbance caused by the roadway excavation, the vertical stress remained approximately 19.0 MPa. Following the excavation of the working face (at which point the measurement points on section A-A were 3 m from the working face, and those on section B-B were 18 m from the working face), a large unloading zone formed in the floor. On section A-A, the measurement point F_D1 on the solid coal side was unaffected by mining activities, and its vertical stress remained unchanged. At points F_D2 on the left side of the roadway and F_D3 in the middle of the roadway, the degree of unloading was relatively low, with stress values decreasing to 18.0 MPa. In contrast, at points F_D4 on the cutting seam side of the roadway

and F_D5 on the gob side, the stress values decreased more significantly to 16.5 MPa. During this excavation step, since the monitoring section B-B was located far from the working face, the stress values at all measurement points on this section remained unchanged. At 4.5 days, the working face advanced into its second excavation step, and section A-A entered the roadway-retention stage. At this point, the stress readings at all monitoring points declined; however, the reduction at F_D1 was marginal, since the solid-coal side had not yet been influenced by goaf-induced pressure relief. In contrast, the closer F_D2, F_D3, F_D4, and F_D5 lay to the goaf, the greater the pressure relief they experienced, with their stabilised stresses registering 16.0 MPa, 13.0 MPa, 8.0 MPa, and 5.0 MPa, respectively. Meanwhile, the B-B monitoring point remained unaffected. At day 5.75, the working face entered its third excavation phase (at this time, the A-A section monitoring point lay 11 m behind the face, while the B-B point was 4 m ahead). At A-A, the stress at F_D1 rose slightly, owing to stress concentration at the roadway floor corner on the intact-coal side. In contrast, F_D2, F_D3, F_D4 and F_D5 each exhibited modest stress reductions. As the face continued to advance during the roadway-retention period, stresses at all points remained essentially constant, stabilising at 20.0 MPa, 18.0 MPa, 10.0 MPa, 5.0 MPa and 2.0 MPa, respectively. During the third excavation step, the underlying strata at B-B were affected, showing a slight stress drop. In the fourth step, F_D1 first decreased marginally and then gradually recovered to 20.0 MPa, while F_D2-F_D5 mirrored both the magnitude of reduction and the stabilised stresses observed at A-A. After the fifth excavation step, all points except F_D1 underwent further pressure relief, ultimately attaining vertical stress values identical to those at section A-A.

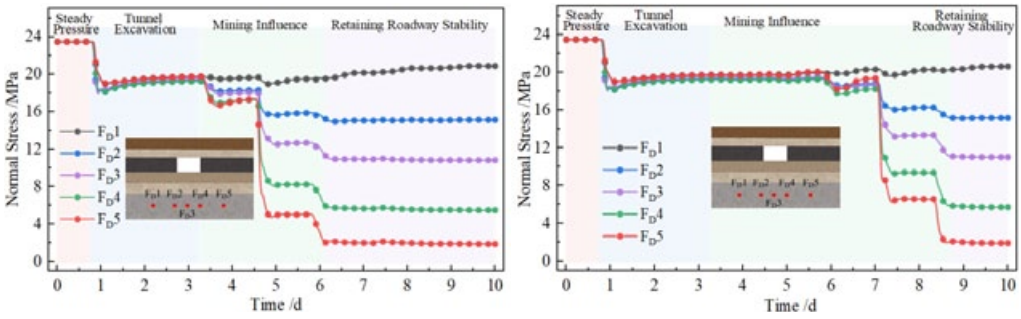

(a) A-A section (b) B-B section

Fig. 9. Stress evolution curve of underlying rock strata

4.2. Analysis of basic bottom stress evolution

The two sets of F_Ci monitoring points are located at the interface between the main floor and the underlying strata. Their number and arrangement are identical to those of the F_Di points, and they serve to monitor the stress state of the main floor during roadway excavation and longwall mining. The variations in vertical stress at these points on both sections are shown in Fig. 10. After roadway excavation, the vertical stress at F_C3 within the entry dropped to 12.0 MPa, while the paired F_C2 and F_C4 points decreased to 14.5 MPa. Both the solid-coal side and the goaf-side exhibited smaller reductions, declining to 19.0 MPa. During the subsequent period of sustained loading, stresses at all points recovered by approximately 1.0 MPa before

reaching a new equilibrium. During the first excavation step of the working face, the A-A section was only weakly affected by mining-induced stress redistribution. At A-A, the vertical stress at F_C1 on the solid-coal side remained essentially constant, while the F_C5 point on the goaf side decreased by approximately 2.0 MPa; the remaining monitoring points showed only slight reductions. The B-B section, being farther from the face, exhibited no noticeable mining-induced stress changes. During the second excavation step of the working face, stress concentration at the foot corner on the solid-coal side caused the F_C1 reading to rise gradually, though only marginally. In contrast, F_C2, F_C3, and F_C4 experienced pronounced pressure relief, stabilising at 13.0 MPa, 7.5 MPa, and 2.3 MPa, respectively. On the goaf side, the F_C5 point underwent instantaneous pressure relief, with vertical stress plummeting to 2.0 MPa. At this stage, the B-B section monitoring point remained unaffected by mining-induced stress changes. During the third excavation stage, the solid coal side stress gradually recovered to the original rock stress level. Along the A-A section, stresses stabilised at 13.0 MPa (coal rib), 6.0 MPa, 1.3 MPa, and 0.2 MPa (gob side) after minor adjustments. Simultaneously, the B-B section began showing mining responses: F_C2-F_C4 stabilised after slight reductions, while F_C5 exhibited a post-decline rebound due to advanced abutment pressure in the immediate floor strata. This differential behaviour highlights the complex stress-structure interactions during excavation. During the fourth excavation stage, section A-A fully transitioned into the roadway retention phase, with complete goaf pressure relief terminating stress redistribution and maintaining constant stress values across monitoring points. Concurrently, section B-B initiated floor pressure relief, where the stress evolution and stabilisation values mirrored the patterns observed in section A-A.

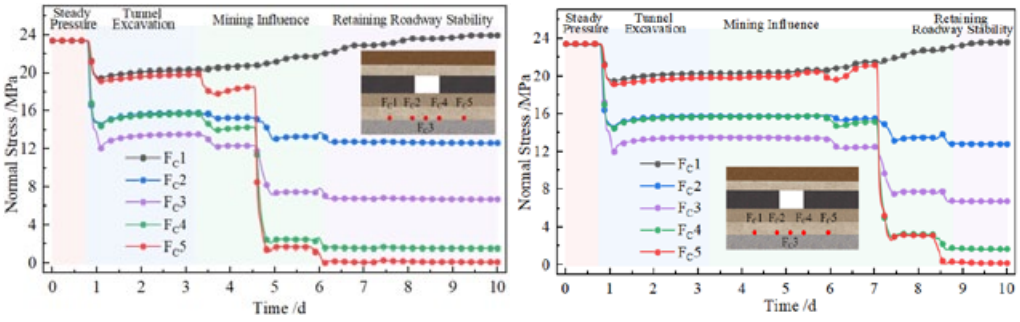

Fig. 10. Stress variation curves of the Basic bottom

4.3. Analysis of direct bottom stress evolution

Seven monitoring points arranged at the interface between the main floor and the immediate floor strata (Fig. 11) were used to track the stress state of the immediate floor. During model pressurisation, the floor hydraulic module was loaded synchronously. After roadway excavation created an unsupported cavity, stress relief occurred instantaneously at the entry and at the left and right rib corners (F_B4, F_B3, F_B5), with stresses dropping from the original in-situ value to 5.0 MPa and 7.0 MPa before stabilising. On both the solid-coal rib side and the goaf side (F_B1, F_B7), stresses initially decreased by approximately 2.0 MPa and then gradually recovered under

stress-concentration effects. The stresses at F_B2 and F_B6 fell to 10.5 MPa and then remained steady. During the first excavation step, the monitoring points lay relatively far from the working face. On section A-A, the F_B1 point showed a continuous stress increase, indicating an intensifying stress concentration at the immediate floor rib corner. The F_B7 point initially dropped by 1.5 MPa before gradually recovering; by the end of this excavation step, both F_B1 and F_B7 had returned to their original in situ stress levels. The remaining monitoring points underwent slight stress reductions before stabilising at new equilibrium values. At this stage, the B-B section remained unaffected by mining-induced disturbance, with all its points maintaining the post-excavation stress values. During the second excavation step of the working face, the stress at F_B1 continued to increase, exceeding the original in situ value and reaching 25.0 MPa, corresponding to a stress concentration coefficient of 1.06. In contrast, F_B2 and FB3, underlain by intact coal roof support showed modest decreases of 1.0 MPa and 1.5 MPa, respectively, before stabilising. The other four points, located within the fractured or plastic zones of the immediate floor, experienced varying degrees of pressure relief due to mining-induced disturbance. Specifically, stresses at F_B4, F_B5, and FB6 dropped by 1.5 MPa, 1.3 MPa, and 7.6 MPa, respectively, yet these points retained partial load-bearing capacity. Meanwhile, F_B7 underwent instantaneous unloading, plummeting from 23.5 MPa to just 0.5 MPa. During the third excavation step of the working face, the immediate floor on section A-A exhibited a largely stable stress regime. The stress concentration at F_B1 continued to grow gradually, ultimately stabilising at 26.5 MPa, corresponding to a concentration coefficient of 1.13 on the solid-coal side. Meanwhile, F_B7 entered its post-peak phase after this excavation step and completely lost its load-bearing capacity. The remaining monitoring points all experienced brief jumps of approximately 0.3 MPa before returning to and maintaining steady values. At this stage, the B-B section began to feel mining-induced disturbances: stresses at F_B1 and F_B7 both intensified, with F_B7 exceeding the original in situ stress to reach 26.0 MPa. All other points on B-B saw slight reductions of around 0.3 MPa before settling into their new equilibrium. During the fourth excavation step, section A-A entered its roadway retention stabilisation phase. The stress concentration beneath the solid coal side floor continued to increase, while readings at all other monitoring points remained unchanged. On section B-B, the F_B7 point on the goaf side underwent instantaneous unloading, with vertical stress dropping sharply from 26.0 MPa to 0.5 MPa; all other points exhibited the same behaviour as observed on A-A. During the fifth excavation step, stress values at all points rose slightly before returning to stable levels, ultimately remaining constant.

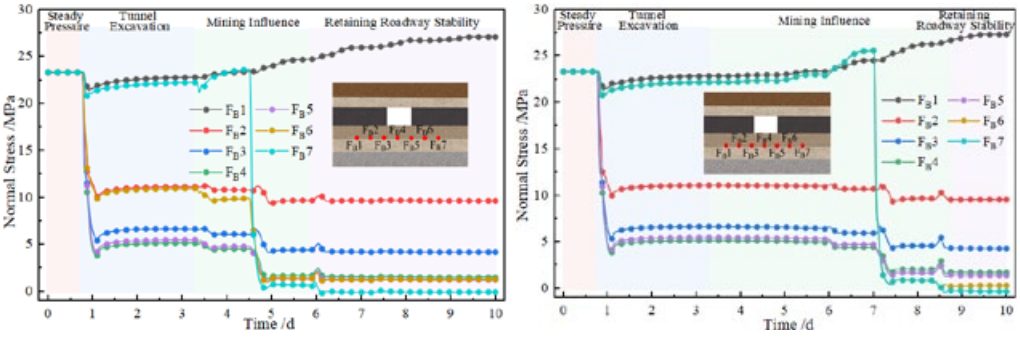

Fig. 11. Stress variation curves of the Direct bottom

4.4. Stress evolution analysis of direct bottom surface

Seven monitoring points were installed on the surface of the immediate floor to track the stress state of the floor plate; their stress variation curves are shown in Fig. 12. Upon roadway excavation, symmetric stress concentration developed along both ribs: F_A1 and F_A7 rose to 27.5 MPa, yielding a stress concentration coefficient of 1.170. In contrast, F_A2 and F_A6 experienced unloading, with stresses falling to 5.0 MPa, though both rib locations retained some load-bearing capacity. The corner and mid-entry points F_A3, F_A4, and F_A5 lying within the fractured zone of the entry underwent instantaneous unloading immediately after excavation, with vertical stresses plummeting to 0.2 MPa and remaining essentially unchanged thereafter. During the first excavation step of the working face, stress concentration at the entry ribs on section A-A continued to intensify, peaking at 30.0 MPa (stress concentration coefficient is 1.28), while F_A2 and F_A6 showed only minor decreases before stabilizing. In the second step, the intact coal side point F_A1 still increased further; F_A2 exhibited a slight, transient rise before returning to its previous level; and on the goaf side, FA6 and F_A7 now exposed to the void suffered instantaneous unloading down to 0 MPa. At this stage, the B-B section remained beyond the influence of mining induced stress changes, although its rib points showed a small uptick in concentration. With the third excavation step, stress concentration on the intact coal side continued to grow, and on section B-B the floor ahead of the goaf reached a maximum of 31.5 MPa (stress concentration coefficient is 1.34). Finally, during the fourth and fifth excavation steps, the intact coal rib monitoring point's stress concentration steadily increased, ultimately reaching 32.0 MPa (coefficient is 1.36), while all other immediate floor surface points maintained nearly constant stress levels.

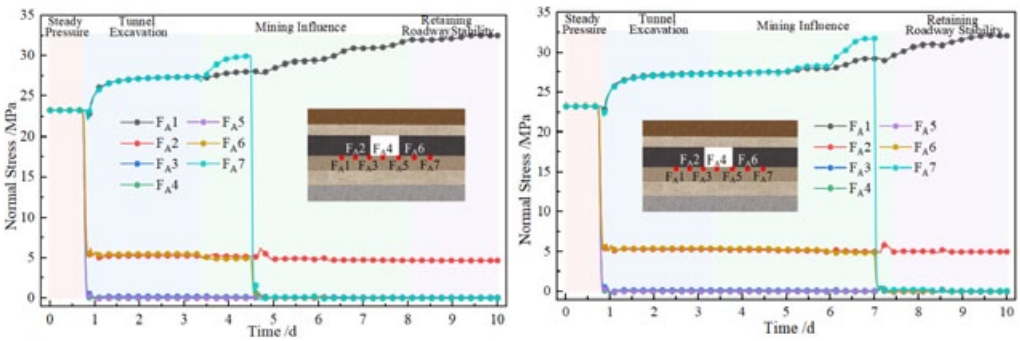

Fig. 12. Stress variation curves of the Direct bottom surface

5. Roof-cutting and initial stress redistribution

5.1. Stress transfer mechanism dominated by overburden fracture and collapse in goaf areas

The disturbance of excavation is small, and there is no obvious deformation of the surrounding rock after roadway excavation and roof-cutting, as shown in Fig. 13(a). When the working face of the upper section was excavated for 7.5 m, the direct roof did not show any obvious

cracks in time, but the separation layer gradually appeared in the process of stability after the excavation, and the amount of separation layer in the middle was the largest, which attenuated to both sides and did not collapse. When the working face is excavated for 15 m, the amount of immediate roof separation increases gradually, and the sinking speed increases. Then, it suddenly collapses along the cutting seam for the first time, forming the initial pressure of the immediate roof. The collapse part is broken into two relatively complete blocks tiled on the floor, and there is no horizontal hinge force between the two blocks. The drop position of the left block is adjacent to the support but not pressed, as shown in Fig. 13(b). When the working face is excavated to 20 m, the immediate roof collapses periodically, and the collapse step distance is about 1/3 of the initial collapse step distance. The overall fracture of the backward immediate roof is three blocks, and the block length on the support side is smaller than the other two blocks. The rock blocks are arranged neatly, and there are transverse through cracks. The hanging space is formed above the block. At this time, cracks appear in the basic roof strata and propagate forward, as shown in Fig. 13(c). After standing for 30 min, the whole block in the middle of the main roof collapses, the block bends, sinks, and vertical tensile cracks appear. The collapsed block on the left side of the goaf has been compacted, and there is a large gap on the right side, which is not completely compacted. The working face was excavated for 35 m, and the immediate roof fell periodically and was paved on the floor of the goaf. The lower part of the basic roof sank and compacted slowly. At the same time, starting from the slit, the upper layer of the main roof appears as a separation layer. The excavation of the working face is 42.5 m, the basic roof collapses periodically, and the periodic weighting step distance is 15 m, which is about 1/2 of the initial weighting, and 1.6 times of the direct roof periodic weighting step distance. After the main roof breaks along the slit, the whole structure is trapezoidal, and the integrity of the block is good. The gangue roadway side is gradually compacted from left to right, and the gangue roadway side is automatically formed to form a common bearing system with the surrounding rock of the roadway, as shown in Fig. 13(d). The working face is excavated for 50 m, and the immediate roof collapses in time. Due to the horizontal extrusion and hinge effect between the blocks, there is a large gap between the middle and lower layers of the main roof, which is curved, and the bottom gangue is further compacted, as shown in Fig. 13(e). When the working face is excavated for 57.5 m, the immediate roof collapses first, and a large range of cracks and voids appear in the main roof. As shown in Fig. 13(f), the whole fracture occurs at 35 m ~ 40 m. The front part of the fracture is affected by the pressure of the overlying rock, and the compaction of the lower gangue is more obvious. The rear part of the fracture is affected by inter-block friction, hinge and so on. It does not compact the goaf, but there are many cracks at the edge, and there are signs of overall collapse. After standing for 30 min, the whole rock strata in the range of 6 m above the main roof bends and sinks on the main roof. The middle part has the largest subsidence and is accompanied by a large number of horizontal and vertical penetrating cracks. The cracks gradually expand along its length, but do not break. According to this, it can be judged that the bearing capacity of the roof's 'short cantilever' beam structure increases at this time, and the pressure of the roadway support increases. The working face is excavated for 65 m, and the immediate roof falls with the mining. The front of the main roof has been compacted, and the rear fracture has not collapsed to the coal wall, which is in the state of a cantilever structure. There is a large suspended space between the contact surface of the immediate roof, and the upper cracks are visibly connected and developed. The subsidence of the upper rock layer is further increased, and the connection with the extension of the slit is still effective, showing an oblique 'F' structure.

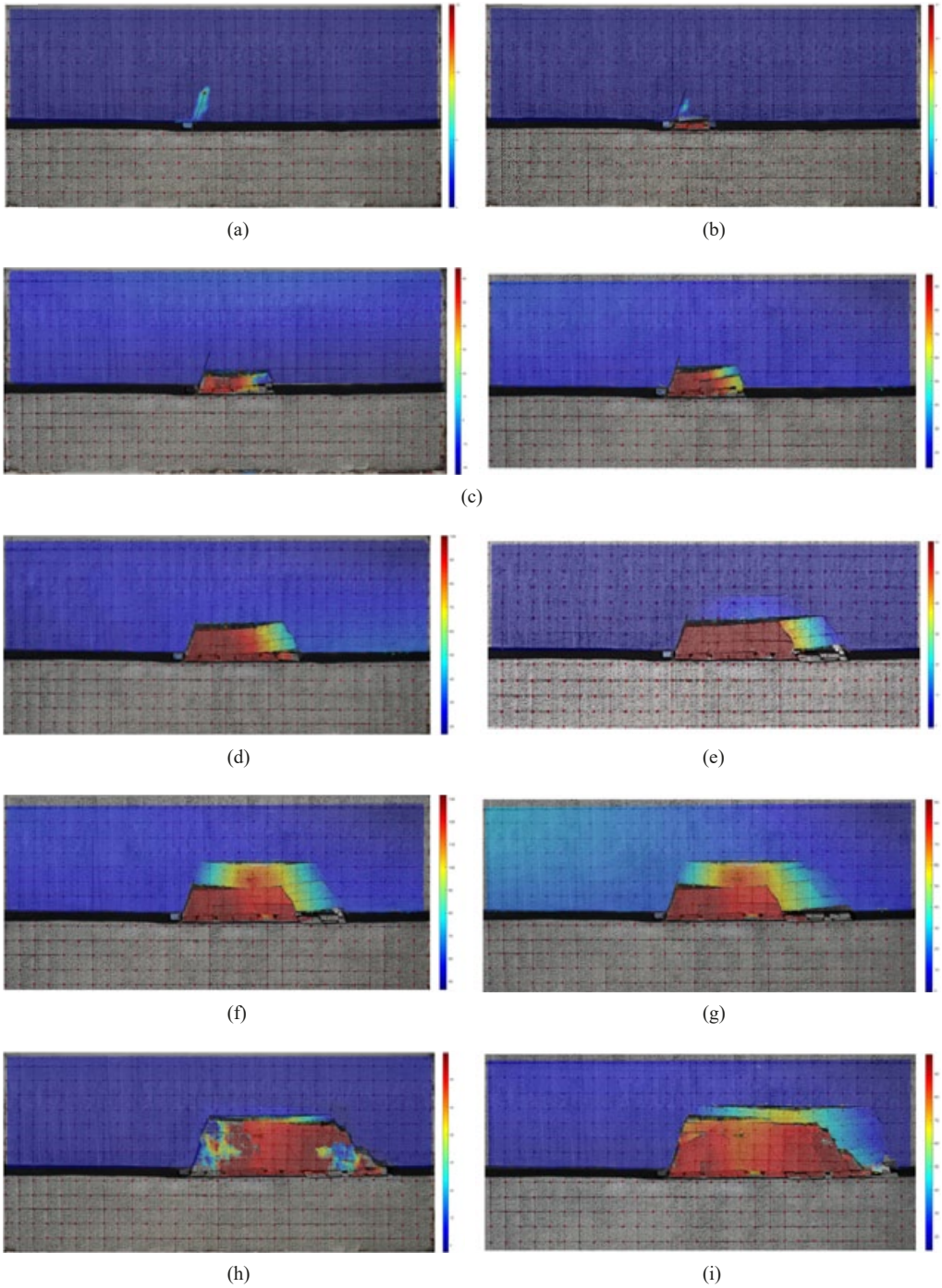

Fig. 13. The caving and migration characteristics of overlying strata in the working face of the upper section of the working face

Its weight is jointly carried by the collapsed basic roof gangue and the key parts of the roof, as shown in Fig. 13(g). When the working face is excavated for 72.5 m, the immediate roof and the basic roof fall almost completely along the cutting seam. The gangue in the goaf is in the form of an oblique trapezoid. At the same time, the interlayer separation is clear, the upper rock fracture is developed, and the filling and compaction effect of the lower part of the goaf is better. The gangue roadway side plays a role in supporting the upper rock layer. The key parts of the roof and the overlying rock layer are in the 'factory' type structure, as shown in Fig. 13(h). When the working face is excavated for 80 m, the upper rock stratum continues to sink, and the middle part is pressed on the lower gangue area. The left and right ends are cantilever structures, respectively, accompanied by fracture development. At the same time, the upper rock stratum appears to show separation, bending subsidence and compaction, as shown in Fig. 14(i). At this point, the mining of the upper section working face is over.

After the excavation of the upper section of the working face, the loading system continues to maintain pressure, and the retaining stage of the engineering site is simulated. Figs. 14(a)-(d) is the evolution characteristics of the overlying rock structure within 48 hours of retaining. After 12 hours after the end of the first mining, the overlying rock gap increases and bends under the action of continuous pressure. Similarly, the central subsidence is the largest, the ends are not effectively disconnected, and it is in the state of cantilever structure. The basic roof gangue near the coal wall side is still not completely broken, leaving a large space and low compactness. As a part of the roadway system, the automatically formed gangue side has a high degree of compaction and plays a major bearing role in the caving gangue in the goaf. After 24 hours of retaining roadway, the gangue near the side of coal wall gradually collapsed and pressed down, and the gangue layer above the basic roof was still not completely collapsed. The main structure of the gangue in the goaf after compaction did not change significantly. The separation and subsidence of the overlying strata at the extension of the cutting seam were obvious, and the overall fracture angle was 75°, which was in a ladder shape. After 36 h of roadway retention, the main structure of the goaf no longer changes, the fracture development, separation and bending

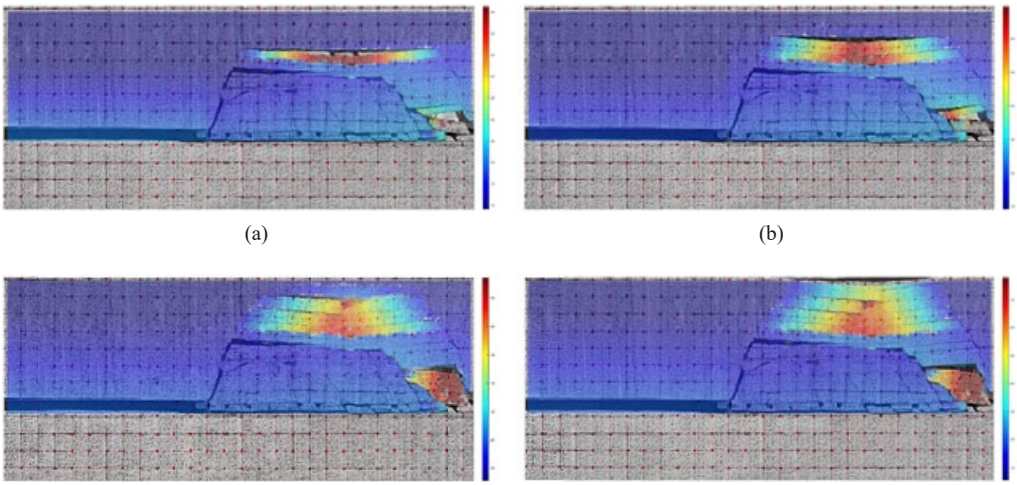

(a) (b)

(a) (b)

Fig. 14. Overburden rock structure evolution characteristics of entry retaining stage

subsidence rate of the upper rock strata begin to gradually decrease, and the slow deformation continues. After 48 hours, the retaining roadway is stable. Limited by the high model, the overlying rock structure no longer changes, the bending subsidence of the upper rock layer is small, accompanied by unpenetrated transverse cracks. The cracks at both ends expand outward along the slit, and there is a separation gap of 1 cm ~ 2 cm at the top. The stable overlying rock caving structure is trapezoidal.

5.2. Stress transfer dominated by roof-cutting 'short cantilever' structure in key parts of the roof

After the roof-cutting, the mechanical connection between the roof of the roadway and the roof of the goaf is broken, and the key parts of the roof above the roadway form the roof-cutting 'short cantilever' beam structure as shown in the Fig. 15. The overburden pressure is transmitted to the floor by the solid coal side, the roadway support body and the compressed gangue side. The cantilever length and the mine pressure of the overlying strata directly determine the size of the force transmitted to the floor, which is the main force source of the floor deformation. Therefore, the evolution of the 'short cantilever' structure (key parts) of the roof during the mining process of the working face is an intuitive manifestation of the stress transfer of the overburden rock, and can also reflect the stress process of the floor. In this section, the author will transfer the analysis of the stress and deformation characteristics of the key parts of the roof 'short cantilever' beam structure to the change of the support and floor force according to the analysis of the stress and deformation characteristics of the key parts of the roof 'short cantilever' beam structure during the collapse of the overburden section.

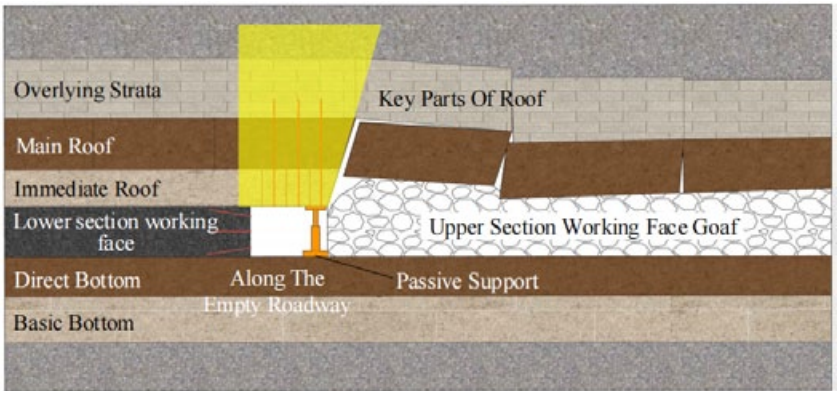

Fig. 15. Structural illustration of 'short cantilever' beam at key position of roof

The advance pre-splitting roof-cutting of the working face eliminates the hanging roof effect caused by the hard rock layer above the roadway, which relieves the mechanical connection between the roadway roof and the partial roof of the goaf, and transforms the 'long cantilever' beam structure of the key part of the roof into the 'short cantilever' beam structure, which reduces the overlying load and rotary deformation force of the cantilever, and reduces the additional force

of the support body in the roadway, which greatly improves the stress environment of the surrounding rock of the roadway. After the mining of the working face, with the periodic collapse and compaction of the goaf, the deformation of the 'short cantilever' beam structure of the roof is also evolving.

The pre-splitting cutting seam breaks the partial connection between the goaf and the roadway roof. The basic roof strata in the goaf are in a critical state of caving. The roof and left boundary of the 'short cantilever' structure are in a fixed constraint state. There is a small compression deformation above the roadway. With the excavation of the working face, the vertical strain of the key parts of the roof changes as shown in Fig. 16(a). The first collapse of the main roof is backward, as shown in Fig. 16(b). The caving gangue fills the goaf, and the roadway side is automatically formed. Due to the fragmentation and expansion characteristics of the gangue, the caving layer of the goaf is similar to the height of the roof-cutting, and the filling rate of the goaf is high, which plays a supporting role in the overlying strata and reaches a certain equilibrium state. Therefore, there is almost no deformation in the key parts of the roof at this stage. The periodic collapse of the main roof is backward. As shown in Fig. 16(c), the connection between the uncollapsed rock strata above the cutting seam and the ' short cantilever ' structure still exists, and as the gangue in the front of the goaf gradually sinks and compacts, the gap between the uncollapsed rock strata and the uncollapsed rock strata gradually increases. Affected by the superposition of the abutment pressure and the lateral abutment pressure of the working face, the uncollapsed rock strata drive the key parts of the roof to rotate and sink to the side of the goaf during the collapse, and the additional load on the support in the roadway increases. The vertical and horizontal displacements of the key parts of the roof during the compaction of the goaf are shown in Fig. 16(d). The mechanical connection within the cutting range is all disconnected, and the rock layer above the main roof is bent and sunken. The maximum subsidence is on the collapsed main roof gangue, and the other end is connected with the key part of the roof to generate a downward rotational deformation force, so that the linkage 'short cantilever' structure is deflected downward. At the

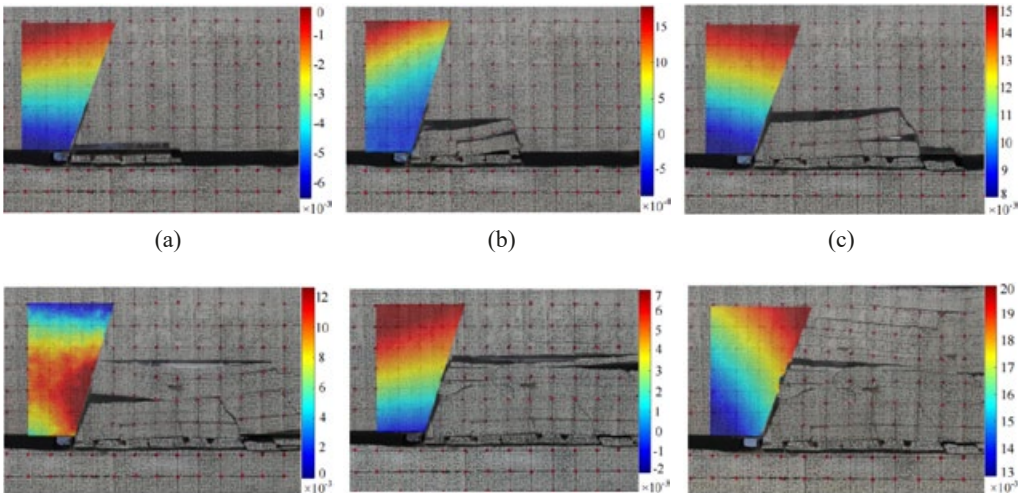

Fig. 16. Vertical strain of key parts of the roof

same time, the upper separation gap increases, and the upper rock layer has a tendency to sink. After the end of the first mining, the 'trapezoid' structure of the overlying rock caving in the goaf is preliminarily formed. As shown in Fig. 16(e), the upper rock fracture is developed and separated, but due to the decrease in the fracture expansion separation gap of the rock, the upper rock layer is supported to a certain extent, and the bending subsidence amplitude is reduced, so the tensile stress on the 'short cantilever' is reduced. During the period of retaining roadway, the influence of mining on the stress evolution of overlying strata is gradually weakened. With the expansion and compaction of gangue in the caving zone, the deformation amplitude of the bending subsidence zone is weakened, and a stable structure with bearing capacity is formed. The change of the rock layer connected to the extension of the slit tends to be stable, the 'short cantilever' rotary subsidence of the roof is gradually in a fixed state, and the stress of the support in the roadway tends to be stable, as shown in Fig. 16(f).

6. Engineering practice

During the mining period of 1452(1) working face in Dingji Mine, the pre-splitting blasting roof-cutting was carried out 30 m ahead of the working face, the roof-cutting angle was 15°, and the height was 13.5 m. As the working face advanced, the roof collapsed in time along the cutting seam and automatically formed the roadway side, and the gangue retaining wall closed the goaf in time to prevent air leakage and water immersion. The roof bolt (cable) in the roadway cooperated with the dense active support of the constant resistance large deformation anchor cable, and the single pillar on the cutting side assisted the passive support to realised the deep gob-side entry retaining. The roadway support form during the mining and retaining of the working face is shown in TABLE 5, and the effect of the on-site roadway retaining is shown in Fig. 17.

TABLE 5

Support Forms in the Lane

	Back timbering	**Ministry support**
Active supporting	Constant resistance large deformation anchorage: φ 21.8×L 13.3 m; Inter-row spacing:1.2 m×1.8 m	Anchor bar: φ 22×L 2.5 m; Inter-row spacing: 0.75 m×0.9 m
	Anchor rope: φ 22×L 6.3 m; Iinter-row spacing: 1.1 m×0.9 m	
	Anchor bar: φ 22×L 2.8 m, Inter-row spacing: 0.84 m×0.9 m	
Passive support	The combined support of three rows of single cantilever shed and stacking support is adopted for 40 m in advance working face.	Row spacing between monomers: 1.2 m×1.8 m
	Within 600 m of the lagging working face, a row of single pillars are used to cooperate with the temporary support of the stacking support.	
	After 600 m of the working face, the I-shaped steel beam is combined with the stacking support to block the gangue support.	

7. Conclusions

(1) Instantaneous pressure relief in the roadway and the roadway after roof-cutting, the degree of pressure relief from the direct bottom to the lower overburden layer is gradu-

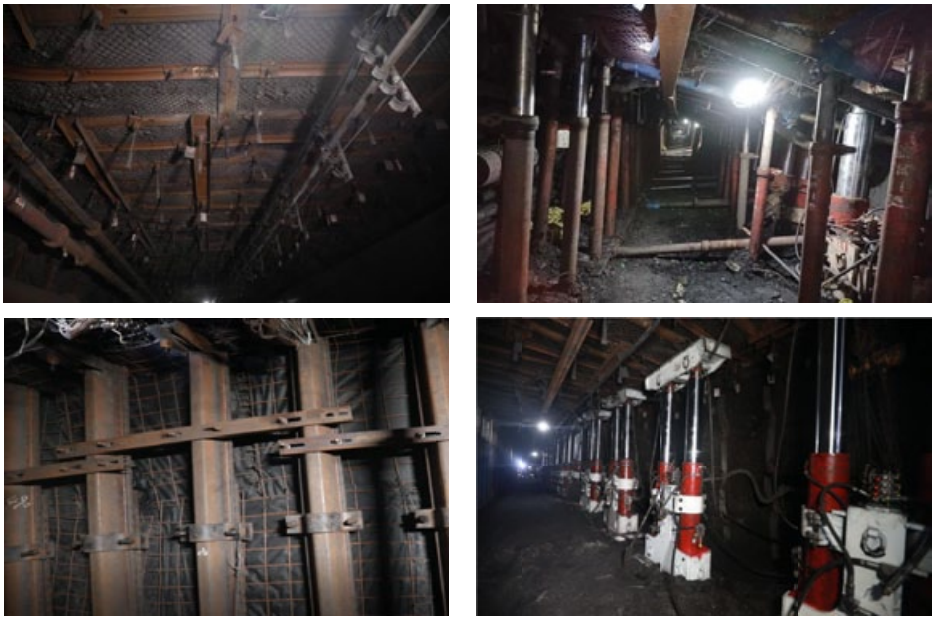

Fig. 17. Lane retaining effect on site

ally reduced, and the reductions are 19.15%, 44.68%, and 74.47%, respectively. In the mining of the working face in the upper section, a high stress zone is formed at 5 m away from the roadway side in the direct bottom layer, and the maximum stress concentration coefficient is 1.34. The high stress is transmitted to the floor through the coal body. The stress on the solid coal side of the basic bottom and the overlying strata recovers to the original rock stress, and the pressure on the goaf side is relieved in a large range, forming an asymmetric stress field. In the early stage of retaining roadway, the overall stress change of floor strata is small; after the stability of the retaining roadway, the stress adjustment of the floor is basically completed, the stress of the solid coal side of the basic bottom layer is restored to the original rock stress, and the stress of the direct bottom layer is concentrated, and the maximum stress concentration coefficient is 1.36.

(2) After the excavation of the working face, the rock strata in the range of the cutting height first collapsed, and the periodic caving steps of the immediate roof and the basic roof were 5 m and 15 m, respectively. Before the goaf is compacted and loaded, the overburden load is mainly carried by the key parts of the coal body and the roof and transmitted to the floor. After the goaf is compacted, the floor fully touches the gangue '*F*' shape structure. The overlying rock finally falls into a 'trapezoidal' caving structure, and the roof caving angle is 75°.

(3) In the early stage of collapse, the goaf cannot bear the load, and the vertical stress is transmitted to the floor through the roof-cutting 'short cantilever 'structure in the key part of the roof, which is manifested as the high tension and low pressure on the cutting side of the key part. As the gangue in the goaf collapses, the upper rock layer does not break the structure, bends, sinks, and separates, causing the key parts of the roof to

rotate and sink. The resulting high additional load is transmitted to the floor through the coal side and the supporting body in the roadway, resulting in an increase in the stress on the floor of the retained roadway. With the periodic fracture and subsidence of the rock layer in the goaf, the key parts of the roof above the slit always experience rotation and compression, so that the force transmitted to the floor has been increasing.

Acknowledgments

All authors contributed to this article. I would like to thank my tutor Professor Xinzhu Hua and Peng Yang for his guidance on this article. Jiyuan Yan modified the manuscript, and the technical guidance provided by Xiao Liu in the engineering site.

Funding

We acknowledge the financial support for this work provided by the National Natural Science Foundation of China (grant No.52374075 and No.51774010), and the Liaoning Provincial doctoral research fund project (2025-BS-0961) for their funding of this work.

References

[1] Y. Zheng, R.L. Shan, B. Huang, et al., Similar model test of strong side and strong angle applied to gob-side entry retaining support. Journal of Mining and Safety Engineering **38** (01), 94-102 (2021). DOI: https://doi.org/10.13545/j.cnki.jmse.2019.0491

[2] H.Z. Zhu, L. Xu, Z.J. Wen, Ground response and failure mechanism of gob-side entry by roof cutting with hard main roof. Journal of Central South University **31**(07),2488-2512(2024). DOI: https://doi.org/10.1007/s11771-024-5695-3.

[3] Heng-Zhong Zhu, Lei-Xu, Zhi-jie Wen, Journal of Central South University **52** (2), 23-33 (2024). DOI: https://doi.org/10.1007/s11771-024-5695-3

[4] H. Wu, Q.F. Li, C.Q. Zhu. He., Study on The Failure Law of Surrounding Rock in Inclined Coal Seam With Gob Side Entry. Scientific Reports **13** (1), 973-973 (2023). DOI: https://doi.org/10.1038/S41598-023-28238-3

[5] Z.Z. Zhang, J.B. Bai, X.Y. Wang, et al., Review and development of surrounding rock control technology forgob-side entry retaining in China Journal Of China. Coal Society **48** (11), 3979-4000 (2023). DOI: https://doi.org/10.13225/j.cnki.jccs.2023.0382

[6] X.Z. Hua, C. Li, X. L. Wang, et al., The deformation mechanism and zoning control technology ofsurrounding rocks of the roof-cutting deep well [J]. Journal of Mining and Safety Engineering **41** (04), 655-665 (2024). DOI: https://doi.org/10.13545/j.cnki.jmse.2023.0189

[7] G.Y. Yu, J. Wang, H. Sun, et al., Floor heave deformation mechanism and comprehensive control technology of block filling gob-side entry retaining. Journal of Mining and Safety Engineering **39** (02), 335-346 (2022). DOI: https://doi.org/10.13545/j.cnki.jmse.2021.0147

[8] Y. Xu, H. Zhou, J.B. Bai, et al., Study on floor heave characteristics and control methods of gob-side entry retaining. Journal of Rock Mechanics and Engineering **34** (S2), 4235-4243 (2015). DOI: https://doi.org/10.13722/j.cnki.jrme.2015.1023

[9] H.S. Wang, M.C. He, J. Wang, et al., Deformation and failure mechanism of gob-side entry in longwa-ll top coal caving face. Journal of Central South University **31** (05), 1542-1559 (2024). DOI: https://doi.org/10.1007/s11771-024-5651-2

[10] G.Y. Yu, J. Wang, H. Sun, et al., Large deformation mechanism and comprehensive control technology of floor heave in gob-side entry retaining with block filling. Journal of Mining and Safety Engineering **39** (02), 335-346 (2022). DOI: https://doi.org/10.13545/j.cnki.jmse.2021.0147

[11] R.L. Shan, Y. Zheng, B. Huang, et al. Li Zhongli, Study on the law of floor heave under the condition of gob-side entry retaining without coal pillar mining in Zhongxing Coal Mine. Coal Engineering **49** (03), 67-70 (2017). DOI: https://doi.org/10.11799/ce201703020

[12] C.C. Yan, G.E. Zhang, T. Chang, et al., Mechanical analysis of floor deformation and floor heave control technology of gob-side entry retaining in shallow buried medium-thick coal seam. Coal Science and Technology **52** (10), 11-20 (2024). DOI: https://doi.org/10.12438/cst.2023–1382

[13] X.Z. Hua, P. Yang, Study on dynamic evolution characteristics of floor deformation of gob-side entry retaining with large section in deep mine. Journal of China University of Mining and Technology **47** (03), 494-501 (2018). DOI: https://doi.org/10.13247/j.cnki.jcumt.000855

[14] X.Z. Hua, M. Yang, Q.J. Liu, et al., Model test study on the evolution mechanism of floor heave in deep gob-side entry retaining. Journal of Mining and Safety Engineering **35** (01), 1-9 (2018). DOI: https://doi.org/10.13545/j.cnki.jmse.2018.01.001

[15] P. Yang, X.Z. Hua, Q.J. Liu, et al., Experimental study on dynamic evolution law of fractal characteristics of floor cracks in large section gob-side entry retaining in deep mine. Rock and Soil Mechanics **38** (S1), 351-358 (2017). DOI: https://doi.org/10.16285/j.rsm.2017.S1.043

[16] H.P. Kang, X. Zhang, D.P. Wang, et al., Control technology and application of surrounding rock in coal pillarless mining. Journal of China Coal Society **47** (01), 16-44 (2022). DOI: https://doi.org/10.13225/j.cnki.jccs.yg21.1940

[17] F. He, W. Zhai, W. Liu, et al., Floor Heave Mechanism and Control Technique of Water-Rich Soft-Rock Roadway in Thick Coal Seam [J]. Energy Science & Engineering **12** (11), 5316-5327 (2024). DOI: https://doi.org/10.1002/ESE3.1956

[18] X.Z. Hua, C. Li, X. Liu, et al., Floor heave mechanism and prevention and control of deep mine roof-cutting entry retaining. Rock and Soil Mechanics **46** (03), 955-968 (2025). DOI: https://doi.org/10.16285/j.rsm.2024.0944

[19] W.F. Xue, S.J. Wang, K.J. Huang, et al., Destruction theory and application of gob-side entry retaining floor with roof cutting in confined water mining area. Coal Science and Technology **45** (S2), 581-588 (2020). DOI: https://doi.org/10.13225/j.cnki.jccs.DZ20.0696

[20] Q. Jiang, Q. Liu, Mechanical similarity distortion mapping principle and case analysis of physical simulation of deformation and failure of underground caverns. Rock and Soil Mechanics **45** (01), 20-37 (2024). D DOI: https://doi.org/10.16285/j.rsm.2023.1254

[21] W.F. Xue, E.K. Hou, S.J. Wang, Floor failure law of gob-side entry retaining without coal pillar cutting. Journal of Xi 'an University of Science and Technology **42** (06), 1133-1139 (2022). DOI: https://doi.org/10.13800/j.cnki.xakjdxxb.2022.0610

[22] J. Chai, Z.C. Han, W.L. Lei, et al., Distributed optical fiber measurement research on the evolution process of floor heave in mining roadway. Coal Science and Technology **51** (01), 146-156 (2023). DOI: https://doi.org/10.13199/j.cnki.cst.2022-1515

[23] X.Z. Hua, C. Li, X. Liu, et al., Current Situation of Gob-Side Entry Retaining and Suggestions for Its Improvement in China. Coal Science and Technology **51** (01), 128-145 (2023). DOI: https://doi.org/10.13199/j.cnki.cst.2022-2082

[24] J.G. Guo, Y.H. Li, S.G. Shi, et al., Self-forming roadway of roof cutting and surrounding rock control technology under thick and hard basic roof. Coal Science and Technology **46** (9), 2853-2864 (2021). DOI: https://doi.org/10.13225/j.cnki.jccs.2021.0790.

[25] C.W. Hu, J.H. Wang, M.C. He, et al., Study on key parameters of self-forming roadway technology without coal pillar in medium-thick coal seam. Coal Science and Technology **50** (04), 117-123 (2022). DOI: https://doi.org/10.13199/j.cnki.cst.2019-0810

[26] H.Z. Zhu, L. Xu, Z.J. Wen, Ground response and failure mechanism of gob-side entryby roof cuttin-g with hard main roof. Journal of Central South University 3**1** (7), 2488-2512 (2024). DOI: https://doi.org/10.1007/s11771-024-5695-3

[27] X.F. Wang, J. Y. Wang, X.Y. Chen, et al., A roadway in close distance to coal seam in deep mine: location selection and supporting practice based on creep characteristics of surrounding rocks. Archives of Mining Sciences **66** (3), 407-419 (2022). DOI: https://doi.org/10.24425/ams.2021.138597